PLASMA WAVES IN JUPITER'S HIGH LATITUDE REGIONS: OBSERVATIONS FROM THE JUNO SPACECRAFT

by

Sadie Suzanne Tetrick

A thesis submitted in partial fulfillment
of the requirements for the Master of Science
degree in Physics in the
Graduate College of
The University of Iowa

December 2017

Thesis Supervisor: Professor Donald A. Gurnett

Graduate College
The University of Iowa
Iowa City, Iowa

CERTIFICATE OF APPROVAL

_____

MASTER'S THESIS

_____

This is to certify that the Master's thesis of

Sadie Suzanne Tetrick

has been approved by the Examining Committee for
the thesis requirement for the Master of Science degree
in Physics at the December 2017 graduation.

Thesis Committee: Donald A. Gurnett, Thesis Supervisor
Jasper S. Halekas, Committee Member
Vincent G. J. Rodgers, Committee Member

ACKNOWLEDGEMENTS

A special thanks to Dr. Donald Gurnett and Dr. Bill Kurth for providing me the opportunity to work on Juno research and for their continued support during the completion of my Master of Science degree. I would also like to thank Masafumi Imai, Jeremy Faden, and Terry Averkamp for their help, feedback, and encouragement that has allowed me to successfully complete this research. A final thank you to my parents, Kelly and Paul Tetrick, my soon-to-be parents-in-law, Rose and Scott Elliott, and fiancé, Josh Elliott for their continued support throughout my educational journey.

ABSTRACT

The Juno Waves instrument detected new broadband plasma wave emissions on the first three successful passes over the low altitude polar regions of Jupiter on Days 240 and 346 of 2016 and Day 033 of 2017. This study investigated the characteristics of these emissions and found similarities to whistler-mode auroral hiss observed at Earth, including the funnel-shaped frequency-time features. The electron cyclotron frequency was much higher than both the emission frequencies for all three days and the local plasma frequency, which was assumed to be ∼20 – 40 kHz. The electric to magnetic field (*E/cB*) ratio was around three near the start of each event and then decreased to one for the remaining duration of each pass. Spin modulation phase shifts were found on two of the three days (Day 240 and Day 033), indicating wave propagation up to the assumed plasma frequency. A correlation of the electric field spectral densities with the flux of up-going 20 to 800 keV electron beams on all three days were found, with correlation coefficients of 0.59, 0.72, and 0.34 for Day 240, Day 346, and Day 033 respectively. We conclude that the emissions are propagating in the whistler-mode and are driven by energetic up-going electron beams along the polar cap magnetic field lines.

PUBLIC ABSTRACT

Since the discovery of Jovian decametric radiation in 1955, it has been known that Jupiter is a powerful source of radio emissions. Early radio measurements detected energetic electrons trapped near the planet's equator, posing serious harm to incoming spacecraft. The Juno spacecraft's Waves instrument is the first radio waves instrument to provide in situ measurements in regions where particle acceleration is present and radio emissions are known to be generated, ultimately providing the first study of Jupiter's polar magnetosphere. This study focused on high latitude plasma wave observations and compared the emissions to plasma wave observations from Earth. This study found that the waves are propagating in the whistler-mode, with similarities to whistler-mode auroral hiss at Earth, based on an analysis of the characteristic frequencies and correlations with up-going electron beams, which are known to generate whistler-mode waves. Overall, these whistler-mode emissions can help better understand the differences between terrestrial and Jovian polar magnetospheres and help determine the location of the local electron plasma frequency, therefore improving density contours in current models of the Jovian system.

TABLE OF CONTENTS

LIST OF FIGURES

Figure

CHAPTER 1

INTRODUCTION

Since the discovery of Jovian nonthermal radio emissions in 1955, it has been known that Jupiter is a powerful source of radio emissions in the decameter wavelength range [*Burke and Franklin*, 1955]. The discovery of Earth's radiation belt in 1958 by James Van Allen [*Van Allen et al.*, 1958] eluded to the idea of a similar radiation belt surrounding Jupiter. One year later, the idea of a Jovian radiation belt was proposed [e.g. *Field*, 1959] and its existence was later confirmed by the Pioneer 10 and 11 spacecraft [*Simpson et al*., 1974*a*; *Van Allen et al*., 1974*b*; *Simpson et al*., 1975; *Van Allen et al*., 1975; *McDonald et al*., 1976]. Even before in situ plasma wave observations were made at Jupiter, the existence of local plasma wave emissions that could not be detected remotely was hypothesized [*Kennel*, 1972; *Thorne and Coroniti*, 1972]. In 1979 the two Voyager spacecraft obtained in situ observations of radio emissions at Jupiter down to hectometer and kilometer wavelengths and discovered close similarities to plasma wave phenomena at Earth. These two spacecraft later discovered similar emissions coming from Saturn, Uranus, and Neptune. A more detailed timeline of the history of Jovian radio emissions can be found in Table 1 of *Carr et al.* [1983].

Because of the strong Jovian magnetic field, highly energetic electrons can become trapped near the planet and pose serious threats to incoming spacecraft, making in situ measurements difficult. What drives many magnetospheric plasma wave studies is to not only identify wave phenomena, but also understand the origin of the waves and their interactions with particles. Studies done on Jupiter are used to compare with both terrestrial and other outer planet magnetospheric plasma waves, such as at Saturn, Uranus, and

Neptune [*Moses et al*., 1990; *Bagenal*, 1992].

The Juno spacecraft is the first mission to pass directly over the low altitude polar regions of Jupiter, taking measurements in regions where particle acceleration is present and radio emissions are known to be generated. Launched on August 5, 2011, the spacecraft arrived at Jupiter on July, 5 2016 and made its first scientific observations of the Jovian polar regions on August 27, 2016 (Day 240 of 2016).

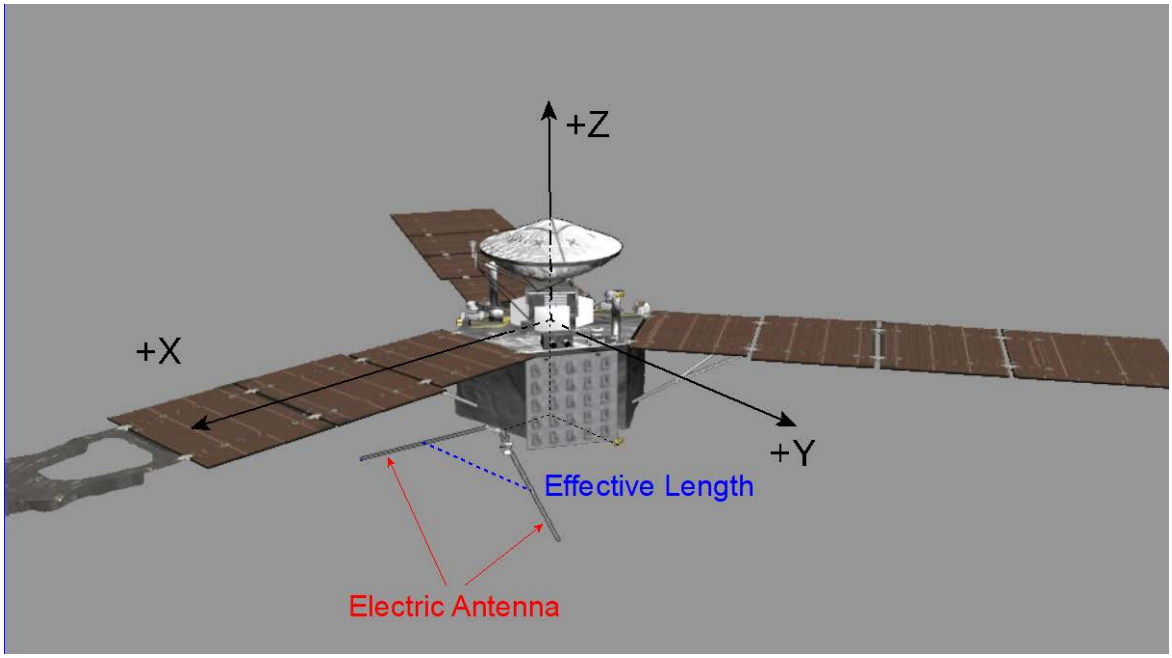

Figure 1. Drawing of the Juno spacecraft, indicating the location of the Waves effective dipole electric antenna (y-axis) and the magnetic search coil antenna (z-axis). The electric antenna is symmetric about the x-axis. Twice per rotation the electric antenna measures the components of the wave electric field approximately parallel and perpendicular to the Jovian magnetic field.

The Juno mission's scientific goals are to explore the origin and evolution of Jupiter, with specific focus on the Jovian polar environment, including the aurora. The scientific objectives of the mission are described in further detail in *Bolton et al.* [2010] and specifically magnetospheric ones by *Bagenal et al.* [2014]. Each of the nine instruments

onboard the spacecraft are designed to explore different aspects of these scientific questions. Because of the extensive instrumentation and unique orbital trajectory of the Juno spacecraft, the mission can address many unanswered scientific questions, specifically ones relating to mechanisms of auroral processes and the interior structure of Jupiter.

Onboard the Juno spacecraft, the University of Iowa's Waves instrument makes measurements of radio and plasma waves. It measures the electric field from 50 Hz to 40 MHz with a single dipole antenna and the wave magnetic field component from 50 Hz to 20 kHz with a search coil magnetometer. The electric antenna's sensitive axis is oriented parallel to the spacecraft y axis (the antenna is in a "V" configuration with effective length approximately equal to 2.4 meters, half of the tip-to-tip length). The search coil magnetometer is oriented with its sensitive axis parallel to the spacecraft spin axis, or z axis, as shown in Figure 1. Both the electric and magnetic spectra are sampled at a rate of once per second. The goal of Juno's Waves instrument is to acquire the data needed to compare the generation mechanisms driving magnetospheric and auroral processes near Jupiter to similar ones observed near Earth. A more detailed description of the Juno Waves instrument can be found in *Kurth et al.* [2017, submitted]. Another Juno instrument used in this study is the Jupiter Energetic particle Detector Instrument (JEDI) which measures energetic electrons and ions, including ion composition and pitch angle distributions of electrons in the energy range of $\sim$25 to 800 keV [*Mauk et al.*, 2017]. Without in situ measurements in Jupiter's high latitude regions it is difficult to relate auroral phenomena to the dynamics of the magnetosphere and ultimately determine their generation mechanisms. The studies done by Juno not only help to support and/or contradict the theories behind such processes, but models of the Jovian magnetosphere can be greatly improved.

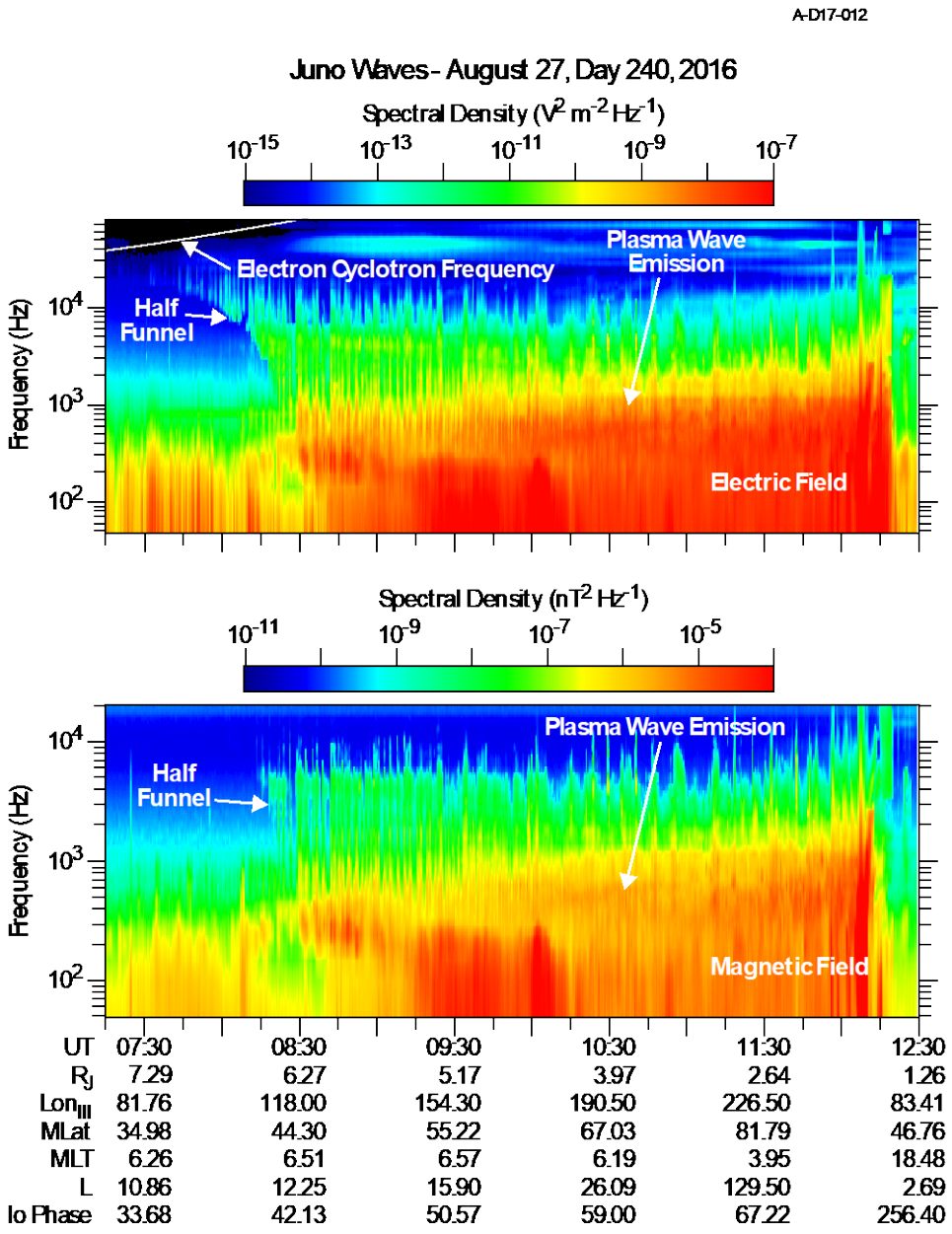

Figure 2. Frequency-time spectrograms of the electric and magnetic field spectral densities on Day 240, corresponding to the first pass over the Jovian northern polar regions. The new plasma wave emission is observed between 07:30 – 12:12 UT in both the electric and magnetic field data. The emission at 12:15 UT is assumed to primarily come from electrostatic waves and not whistler-mode emissions. The white line indicates the location of the electron cyclotron frequency, which is well above the observed emission frequency for the duration of the pass. Adopted from *Tetrick et al.* [2017].

When Juno made its first pass over the low altitude polar regions of Jupiter's magnetosphere on August 27, 2016 (Day 240 of 2016), a new type of Jovian plasma wave emission was observed that had never been seen before. Frequency-time spectrograms of the electric and magnetic field spectral densities of this new emission are shown in Figure 2. The plasma wave emission is labeled in Figure 2 and consists of the predominately bright-red region in both the electric and magnetic fields. The Juno spacecraft is in a 53-day orbit, meaning it has a Perijove (PJ), or closest approach to Jupiter, every 53 days. As of the writing of this thesis, Juno has made three passes over the high latitude regions of Jupiter with its science payload powered on. Perijove 1 (PJ1) on August 27, 2016, Perijove 3 (PJ3) on December 11, 2016 (Day 346 of 2016), and Perijove 4 (PJ4) on February 2, 2017 (Day 033 of 2017). No data was obtained during Perijove 2 due to a shift to a safe-mode because of an on-board software issue. The same type of plasma wave emission detected on Day 240 was also seen on the other two passes (Day 346 and Day 033). Figure 3 shows the electric field spectrograms for all three days. This study investigates the characteristics of these plasma wave emissions in order to establish the mode of propagation and the possible mechanisms by which they are generated.

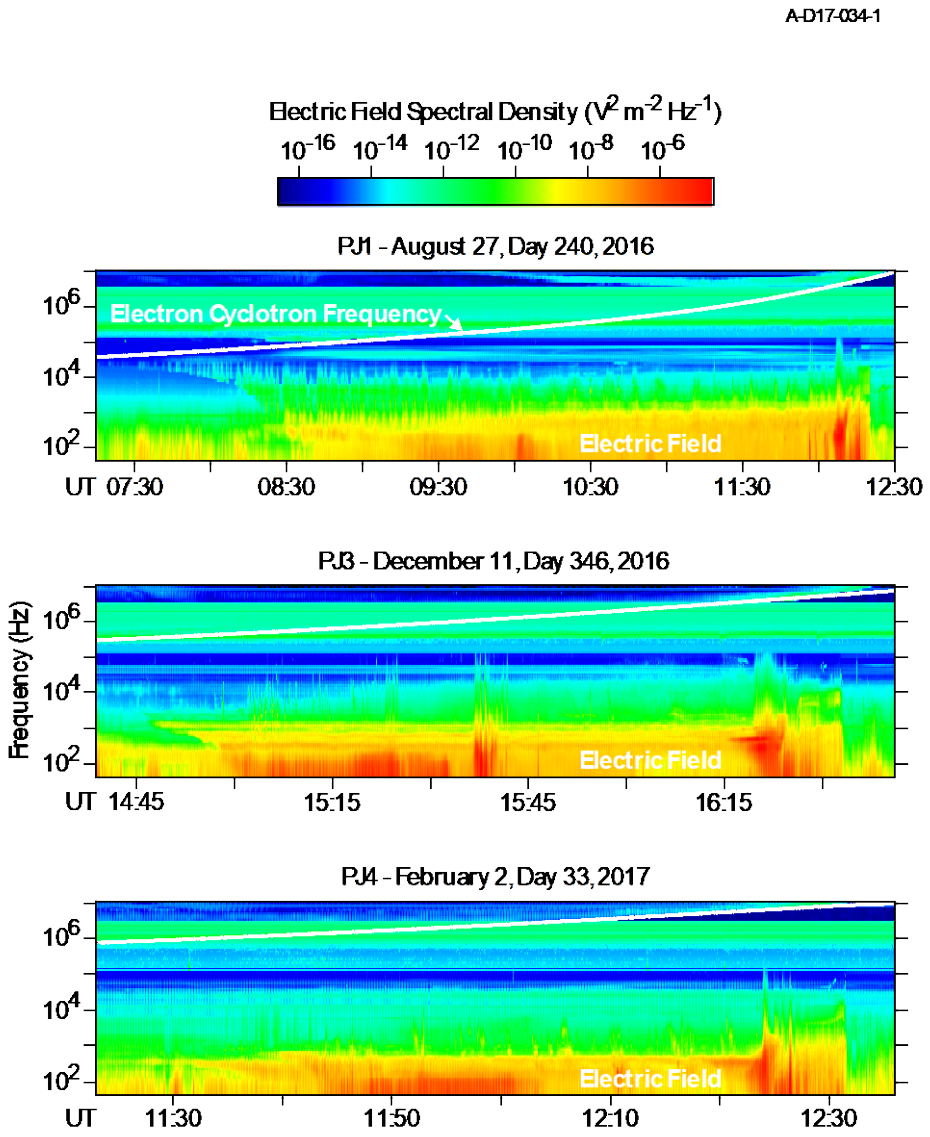

Figure 3. Frequency-time spectrograms of the electric field spectral densities on Day 240 (top panel), Day 346 (middle panel), and Day 33 (bottom panel). Half-funnel-shaped emissions occur on all three days when the Juno spacecraft passes over the northern polar regions. The white line indicates the location of the electron cyclotron frequency, which is well above the observed emission frequencies for all three days.

CHAPTER 2

THE JOVIAN SYSTEM AND JUNO'S TRAJECTORY

As was noted in Chapter 1, early radio measurements provided insight into the Jovian magnetospheric environment. Some of the key differences between Jovian and terrestrial magnetospheres should be discussed to gain a better understanding of the Jupiter system. The first notable difference is the size of the planets and their respective magnetospheres. Jupiter is approximately ten times the diameter of Earth, and the Jovian magnetosphere, determined by both the strength of the magnetic field and the distance from the sun, is also much larger than the terrestrial magnetosphere. Jupiter is farther away from the sun than Earth so the solar wind ram pressure is much lower therefore increasing the size of the magnetosphere. The solar wind and the ionosphere are the dominant sources of plasma at Earth, while the Jovian system contains the satellite Io, which produces volcanic plumes that are the main source of plasma in the Jovian magnetosphere. The magnetosphere of Jupiter also encompasses a total of 4 large moons (called Galilean satellites), whereas the Earth's moon is located outside its magnetosphere. Lastly, a big factor in the Jovian magnetospheric system is the strong centrifugal forces of the rapidly rotating planet. Due to the sheer size and rapid rotation of Jupiter's magnetosphere, the rotation provides the dominant source of energy to drive magnetospheric phenomena. This is very different from Earth, where the interaction with the solar wind is thought to be the dominate driver of terrestrial magnetospheric phenomena. Figure 4 shows a cartoon image of the magnetosphere of Jupiter, which extends approximately 63 – 92 Jovian radii on the sunward side (where 1 Jovian radii, or R_J = 71,492 km [*Bagenal et al.*, 2014]), and extends beyond 4 AU on the tail-ward side. Although there are many differences between Jovian and terrestrial

magnetospheres, auroral-related phenomena are thought to have similar processes. However, without in situ measurements at high latitudes, it is difficult to relate the observed aurora to the dynamics within the Jovian magnetosphere and ultimately compare these observations to terrestrial ones. To this day, many of the ideas behind processes that generate the aurora at

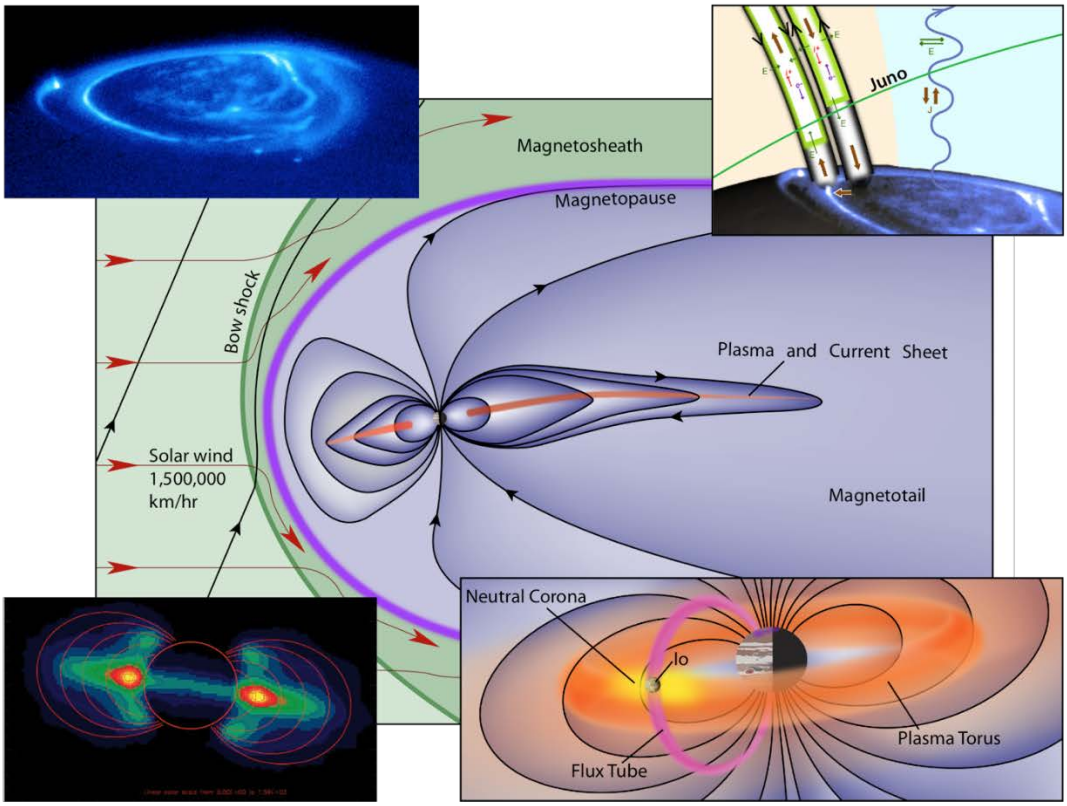

Figure 4. All figures adopted from *Bagenal et al*. [2014]. (**Middle**) Cartoon image of Jupiter's magnetosphere, showing the interaction with the solar wind and location of the plasma and current sheet. (**Top left**) Image of auroral emissions at Jupiter. (**Top right**) Showing how Juno will fly through the regions where particles are known to be accelerated. (**Bottom right**) Showing the location of Io and the toroidal cloud formation around Jupiter due to the volcanic gases, creating a source of plasma. (**Bottom left**) Image depicting the radiation belts with energetic (MeV) electrons.

Jupiter are based on observations from Earth. Hence, the daunting question for Jovian magnetospheric physics is whether or not the high-latitude structure of the magnetosphere is different than at Earth and if the theories dealing with auroral processes are consistent with Jovian observations.

Juno is the first spacecraft to pass through the high latitude regions, allowing the Waves instrument to take measurements of the electric and magnetic fields. Juno is in a polar orbit around Jupiter, illustrated in Figure 5, which shows the trajectory of PJ1, PJ3, and PJ4 in a magnetic coordinate system aligned with the approximate 9.5 degree tilt of Jupiter's dipole. The time periods of interest are indicated by red lines. Juno "threads the needle" inside its tenuous rings, passing through the radiation belts and therefore minimizing the harm done to the spacecraft. However, the orbit precesses due to the rotational flattening, or oblateness, of the planet, causing the equatorial crossings to become closer per orbit by about 0.9 R_J [*Bagenal et al*., 2014] and eventually crossing through the radiation belts in later orbits. In each perijove, both the northern and southern polar regions are crossed by the inbound and outbound trajectories respectively. The precession of the spacecraft trajectory allows Juno to both sample the structure along the magnetic field (when moving approximately parallel to a magnetic L-shell), and also measure latitudinal structure (when moving over a variety of latitudes). For the current study, all of the perijoves discussed pertain to times where the altitude is varying quite a bit over the observational periods and the precession of the orbit is minimal.

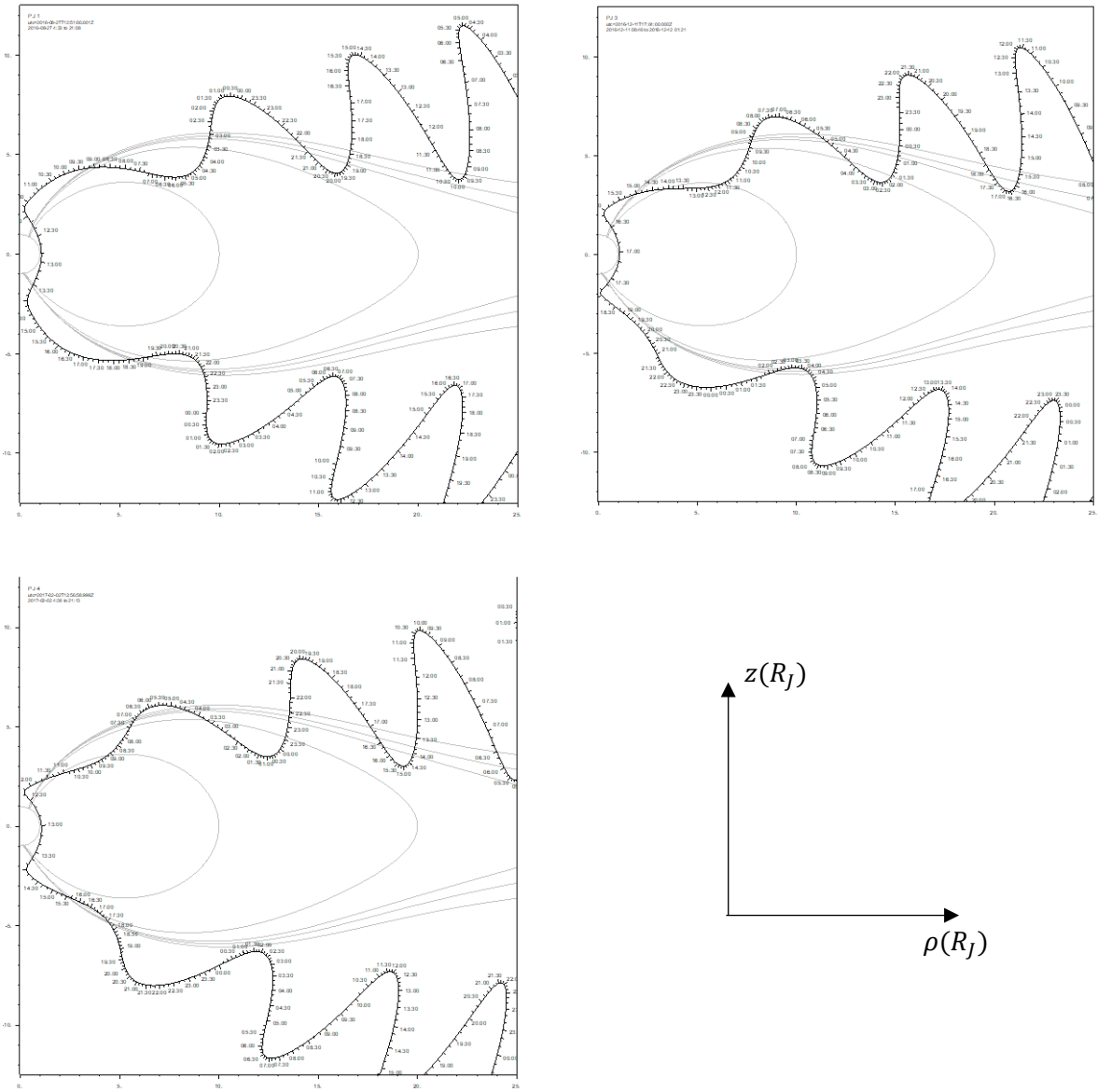

Figure 5. Orbits of PJ1 (top left), PJ3 (top right), and PJ4 (bottom) ("wiggling" black lines) are shown in a magnetic coordinate system that is aligned with the 9.5-degree tilt of Jupiter's dipole. The magnetic field model used to simulate field lines, shown in a magnetic meridian plane, (represented by thin black lines) is the VIP4 model by *Connerney et al.* [1998]. In this coordinate system, the spacecraft "wiggles" due to the tilt of the dipole. The highlighted red regions indicate the time periods that our plasma wave observations were made for each pass. Tick marks are indicated for every 30 minutes. The z-axis is the axis of the dipole of Jupiter and the ρ-axis is distance from the planet (both measured in R_J).

CHAPTER 3

WHISTLER-MODE BACKGROUND AND THEORY

Later in this study, we argue the plasma wave emissions observed by Juno are propagating in the whistler-mode. Therefore, it is useful to first review the background, theory, and characteristics of whistler-mode plasma wave emissions, particularly auroral hiss, in order to understand the arguments made in favor of whistler-mode propagation. Although Jupiter's magnetosphere differs from Earth's, similar observations of whistler-mode plasma wave emissions have been detected, such as the characteristic funnel-shape frequency-time spectrogram of auroral hiss [*Gurnett et al.,* 1979]. Whistler-mode auroral hiss is observed in the high latitude regions of planetary magnetospheres. The emissions were first discovered when low frequency broadband wave emissions were detected via ground-based instruments [*Martin et al.,* 1960]. It was later realized that the emissions were associated with the visible aurora. Following the initial discovery, satellites made observations of whistler-mode emissions at Earth throughout the 1960s and early 1970s [*Gurnett and O'Brien*, 1964; *Gurnett*, 1966; *McEwen and Barrington*, 1967; *Laaspere et al.*, 1971]. Not only have the emissions been detected at Earth but auroral hiss has been found at Jupiter as well, with Voyager 1 making its first auroral hiss observations at Jupiter in the 1970s, which was first analyzed by *Gurnett et al.* [1979]. The source of these emissions was found to be located around an L-value of about 5.6, near the Io plasma torus. Io, one of Jupiter's moons, was found to highly affect radio emissions coming from Jupiter [*Bigg*, 1964]. More recent studies done on Jupiter, via the Ulysses spacecraft, have detected whistler-mode emissions originating in high latitude regions [*Farrell et al.*, 1993]. Similar whistler-mode auroral hiss emissions have also been detected near the rings of Saturn by the

Cassini spacecraft [*Gurnett et al.*, 2005].

The theory behind whistler-mode plasma wave emissions is relatively well understood. The waves propagate at frequencies below both the cyclotron frequency and plasma frequency and have an upper frequency limit at either the cyclotron frequency or plasma frequency, whichever is lower. When whistler-mode auroral hiss emissions are observed on a frequency-time spectrogram a characteristic funnel shape is observed. The funnel shape is due to whistler-mode propagation at wave normal angles near the resonance cone, causing the ray path to increasingly deviate from the magnetic field direction as the frequency increases [*Gurnett*, 1966; *Smith*, 1969; *Mosier and Gurnett*, 1969; *James*, 1976].

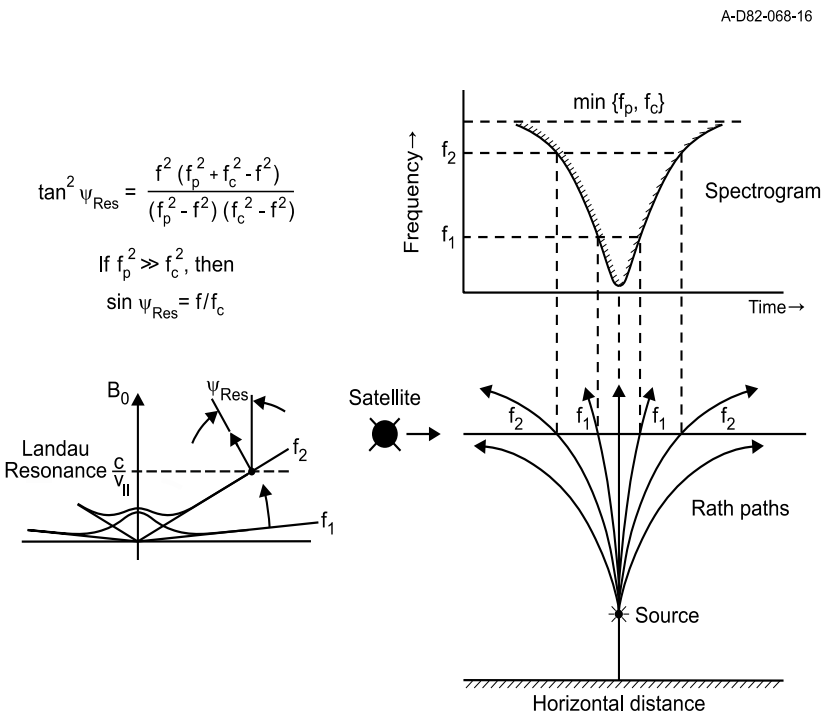

Figure 6. Whistler-mode propagation along the resonance cone. The left two figures depict the resonance cone at two frequencies and the limiting group velocity angle, ψ_{res}, is visually and computationally shown. The right two figures show the frequency-dependence of the wave propagation in relation to the spacecraft moving through the source region. The spacecraft detects higher frequencies first, then the lower frequencies later in time for the left-facing funnel. The opposite is true for the right-facing funnel.

The resonance cone is defined as the region were the index of refraction goes to infinity [*Stix*, 1962; *Gurnett and Bhattacharjee*, 2005]. In this region, where the index of refraction becomes infinite, the group velocity of the wave becomes perpendicular to the resonance cone. Figure 6 shows that as the k-vector, or the direction of wave propagation, deviates further from the magnetic field direction it approaches an angle, the resonance cone angle, where the index of refraction attends to infinity [*Gurnett and Bhattacharjee*, 2005]. The group velocity angle has a limit, called ψ_{res}, shown in the left side of Figure 6. The right image in Figure 6 shows a representation of a frequency-time spectrogram for whistler-mode wave propagation. As the spacecraft passes through an auroral hiss source region, the higher frequencies are detected first and the lower frequencies are detected later in time (for the left-facing funnel; the opposite is true for the right-facing funnel), ultimately creating what looks like a funnel on a frequency-time spectrogram.

Whistler-mode plasma wave emissions have several characteristics that distinguish them from other modes of propagation. Many of these characteristics are caused by propagation near the resonance cone. One characteristic is the quasi-electrostatic property of the emission near the resonance cone, where the wave electric field becomes more parallel to the wave vector. Another distinction, as stated earlier, is the frequency dependence of the resonance cone angle, appearing as a funnel shape on a frequency-time spectrogram because the angle decreases with increasing frequency. Lastly, terrestrial studies of whistler-mode auroral hiss emissions have been found to correlate with field-aligned electron beams [*Gurnett*, 1966; *Gurnett et al.*, 1971; *Gurnett and Frank*, 1976; *Lin et al.*, 1984; *Gurnett et al.*, 1986; *Ergun et al.*, 2003]. The characteristics of the emissions

detected by Juno Waves on Day 240, Day 346, and Day 033 will be analyzed and compared with these common characteristics of whistler-mode auroral hiss emissions in order to conclude with enough confidence whether or not the emissions are propagating in the whistler-mode.

CHAPTER 4

WAVE CHARACTERISTICS AND MODE OF PROPAGATION

To determine if the plasma wave emissions are propagating in the whistler-mode, we need to analyze the characteristics of the waves. As explained in the previous section, whistler-mode waves have several characteristics that distinguish them from other modes of propagation, many of which are due to propagation near the resonance cone. Some features that will be analyzed in the following section include: characteristic frequencies of the wave, such as the electron cyclotron frequency and the electron plasma frequency, the electric to magnetic field ratio, and spin modulation in the electric field.

4.1: CHARACTERISTIC FREQUENCIES

First we analyze the characteristic frequencies of the new plasma wave emissions, represented in frequency-time spectrograms of Figure 2 and Figure 3. The white lines in each illustration represent the electron cyclotron frequency, which is determined by the Magnetometer instrument (MAG) by utilizing a pair of tri-axial Fluxgate Magnetometers (FGMs) to provide magnetic field measurements at sample rates up to 64 vector samples/s [*Connerney et al*., 2017]. The electron cyclotron frequency (in Hz) is then calculated using the total measured magnetic field and the following equation from *Gurnett and Bhattacharjee* [2005], where *B* is in nT:

$$f_{ce} = 28B$$

The emission on Day 240 starts around 07:30 UT and lasts until 12:12 UT (as shown in Figure 2). Similar plasma wave emissions were also detected on PJ3 (Day 346) and PJ4 (Day 033). Figure 3 shows the electric field spectral densities for all three days. Like the

emission observed on Day 240, the Day 346 and Day 033 emissions are also seen in the magnetic field, although these spectrograms are not shown, indicating that all three emissions must be electromagnetic waves. The emission on Day 346 starts around 14:45 UT and lasts until about 16:25 UT. On Day 033 the emission begins around 11:23 UT and ends around 12:35 UT. Figure 7 shows Juno's trajectory for all three days, where the red/purple highlighted regions indicate the time periods of the spectrograms from Figure 3. During each time period Juno passes over a wide range of the Jovian polar cap region, including the main auroral oval (represented as a black oval). The red and black dots indicate the start and end times of the lower frequency cutoffs of each emission. The significance of these dots in relation to the auroral oval will be discussed later.

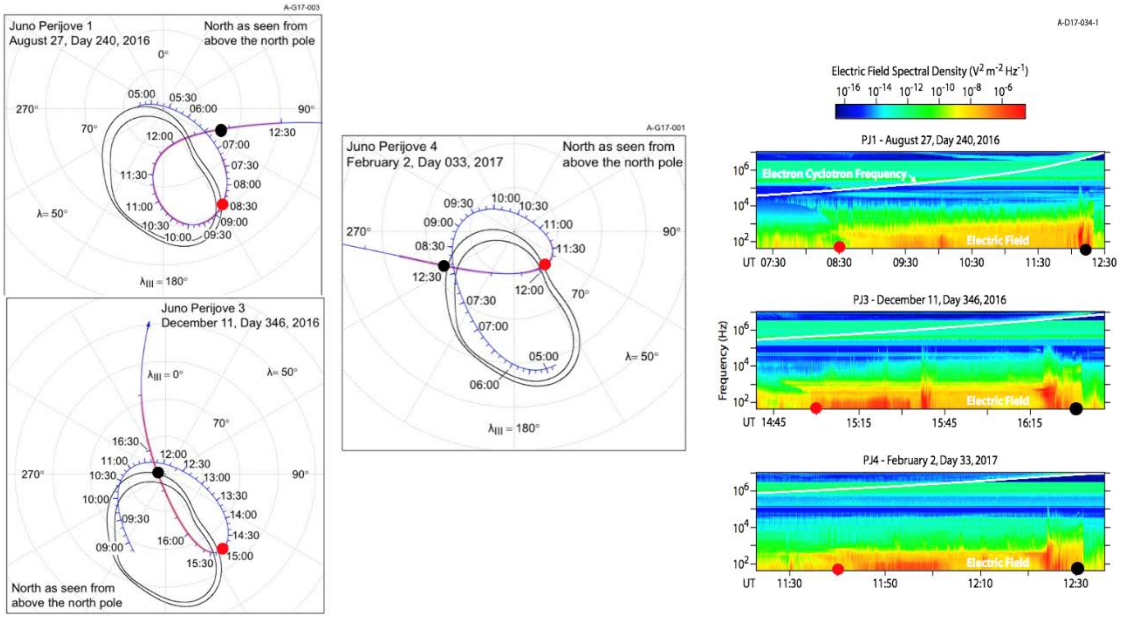

Figure 7. Left three images show plots of the trajectory of Juno (blue line) on Day 240 (top left), Day 346 (bottom left), and Day 033 (right). Shows the magnetic projection onto Jupiter using the VIP4 magnetic field model [*Connerney et al.*, 1998]. For the duration of the observed emissions, the spacecraft passed over the statistical auroral oval based on Hubble UV observations (black ovals) and the northern polar cap region of Jupiter for all three days. The red/purple lines represent the same time intervals of the spectrograms for each emission (image shown on right). The red dots indicate the lower-frequency cutoffs at the start of each emission and the black dots indicate the

lower-frequency cutoffs at the end of each emission. These dots also indicate when JEDI observed intensifications in up-going electron fluxes, corresponding to the boundaries of the statistical auroral oval.

A high-maximum detectable frequency of each emission is seen in Figure 3. For both Day 240 and Day 346 this maximum frequency occurs at about 20 – 40 kHz throughout the duration of the emission, increasing slightly near the end. In contrast, on Day 033 the maximum detectable frequency is about a factor of ten lower than the first two days, occurring around 2 kHz throughout the duration of the pass, but also increases near the end up to about 20 kHz. It should be noted that there are no clear cutoffs in frequency for any of the three days in either the electric or magnetic field, but rather gradual decreases occur until the wave intensities are no longer detected. The reason why the maximum detectable frequencies are higher for the electric field as compared to the magnetic field (see Figure 2 for Day 240), is due to the better sensitivity of the electric field antenna; the observed frequencies run into the noise level of the magnetic field before the electric field. All three days also have lower-frequency cutoffs that are time-dependent. The lower-frequency cutoffs occur at both the start and end of all three emissions (as shown by the red and black dots in Figure 7), although this is less prominent near the end. This shape is reminiscent of funnel-shaped whistler-mode auroral hiss emissions observed at Earth over the auroral region [*Gurnett et al.*, 1983], but with half of the funnel facing left near the beginning of the emissions, and the other half of the funnel (but with less curvature) near the end of the emissions.

The relationship of the electric and magnetic field spectrums to the electron cyclotron frequency, ω_c, and electron plasma frequency, ω_p, provide vital clues for

establishing the mode of propagation. First, we will consider the electron cyclotron frequency, which begins at ~40 kHz for Day 240, ~400 kHz for Day 346, and ~800 kHz for day 033 at the start of each pass. These frequencies then increase to ~10 MHz for all three days near the end of each pass (see the white lines in Figure 3). The frequencies of the plasma wave emissions are lower than the electron cyclotron frequencies on all three days for the entire duration of each pass. The very large cyclotron frequency provides a highly different magnetospheric environment than is typical over Earth's polar region, where the cyclotron frequency is usually much closer to the frequencies of whistler-mode auroral hiss emissions.

Next, we consider the relationship of the observed emission frequencies to the electron plasma frequency. Unfortunately, over the polar regions of Jupiter there is no clear indication in the Waves data of the local electron plasma frequency for any of the three passes. As was stated earlier, whistler-mode emissions can only propagate below the electron cyclotron frequency or the electron plasma frequency, whichever is lower. Because of this, we have assumed that the plasma frequency is slightly above the maximum detectable frequency of each emission, i.e. around 20 – 40 kHz. We interpret the other narrow-band emissions observed above these assumed plasma frequencies (as seen in Figure 3) as ordinary mode radio emissions, which would also be consistent with the plasma frequencies we have estimated.

4.2: ELECTRIC TO MAGNETIC FIELD RATIO

An important factor in identifying the mode of propagation is the electric to magnetic field ratio (*E/cB*) where *c* is the speed of light. Since whistler-mode emissions become quasi-electrostatic ($E \gg cB$) when the wave is propagating near the resonance cone, this results in $E/cB > 1$ [see *Gurnett and Bhattacharjee*, 2005]. Figure 8 shows the observed color-coded (*E/cB*) ratios for all three passes. As can be seen the (*E/cB*) ratios near the start of the left-facing half funnel-shaped emissions (08:00 – 08:30 UT for Day 240,

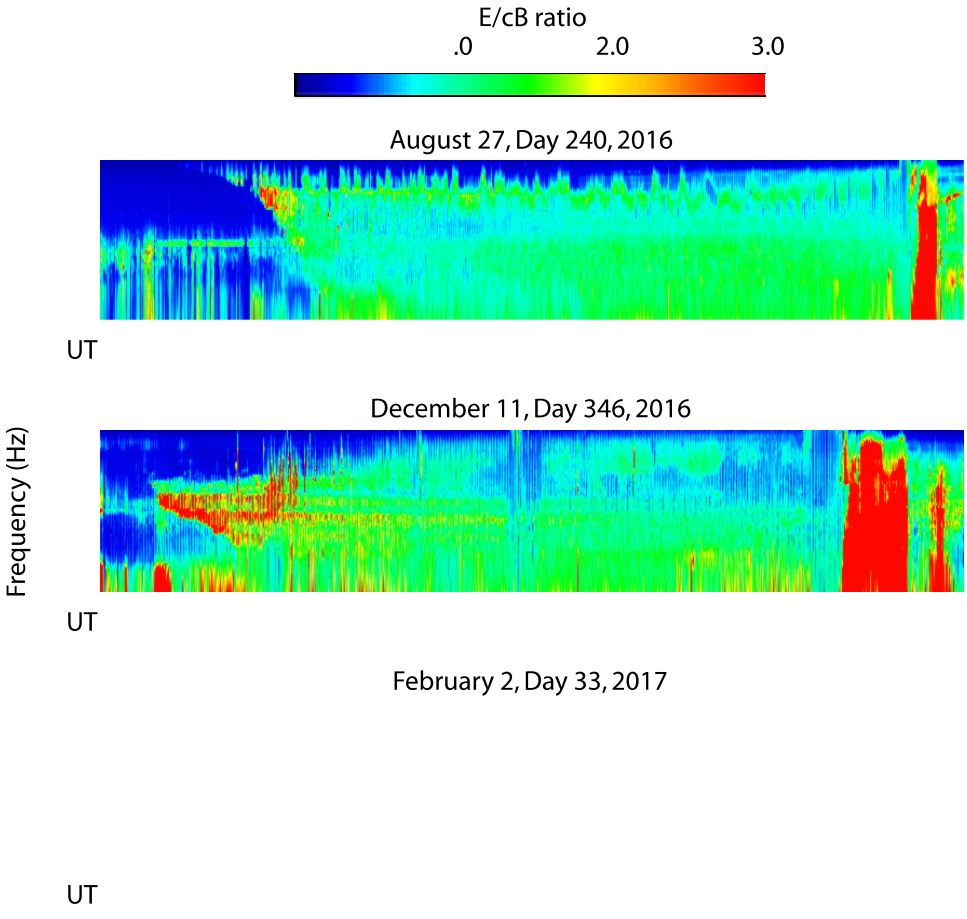

Figure 8. Frequency-time spectrograms of the E/cB ratio for Day 240 (top panel), Day 346 (middle panel), and Day 033 (bottom panel). The ratio is about three at the start of each pass, then decreases to one for the rest of the passes. The region with a large ratio around the end of each pass (around 12:15 UT for Day 240) is thought to be primarily due to electrostatic waves and not whistler-mode emissions.

14:45 – 15:10 UT for Day 346, and 11:30 – 11:45 UT for Day 033) are approximately three. An (*E/cB*) ratio significantly greater than one strongly supports the idea that the mode of propagation is whistler-mode. Although it should be noted that this value is not as high as sometimes occurs for whistler-mode propagation near the resonance cone, the fact that the *E/cB* ratios are relatively modest is likely due to the emissions not extending all the way up to the plasma frequency where *E/cB* approaches infinity. After the beginning of the emissions, the (*E/cB*) ratio decreases to about 1.0 to 1.5 for the rest of each pass. That whistler-mode *E/cB* ratios can be as small as one can be seen from the following equation which gives the index of refraction, $n \cong cB/E$, for parallel propagating, i.e. $\theta = 0$, right-hand polarized whistler-mode waves [*Stix,* 1962]:

$$n^2 = 1 - \frac{\omega_p^2}{\omega(\omega - \omega_c)}$$

Note that when the cyclotron frequency becomes much larger than the plasma frequency, $\omega_c \gg \omega_p$, the second term after the equal sign becomes very small, much less than one. This causes the value for n to be nearly one, which means that $(E/cB) \approx 1$. Of course, at larger wave normal angles, the *E/cB* ratio can become greater than one, eventually approaching infinity at the resonance cone.

4.3: ELECTRIC FIELD SPIN MODULATION

Spin modulation measurements also provide another important tool for determining the mode of propagation. The Juno spacecraft is spin-stabilized and rotates in the right-hand sense around the axis of the spacecraft high gain antenna which is defined to be the +z axis (see Figure 1). The spin period is 30 seconds. Because of the need to transmit data via the high gain antenna, the +z axis normally points toward Earth. As was stated

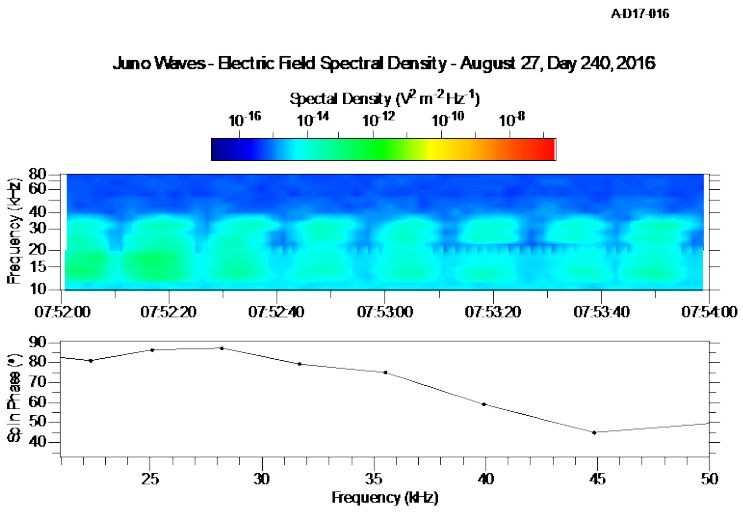

Figure 9. Top panel shows the electric field spectral density near the start of the emission on Day 240, depicting spin modulation in the electric field. The bottom panel shows the spin phase of the maximum electric field relative to the planetary magnetic field, 0 degrees representing $E \parallel B_0$, and 90 degrees representing $E \perp B_0$. The frequency-dependence in the spin phase can be seen. At lower frequencies $E \perp B_0$ and as frequency increases, the electric field becomes almost parallel to the planetary magnetic field.

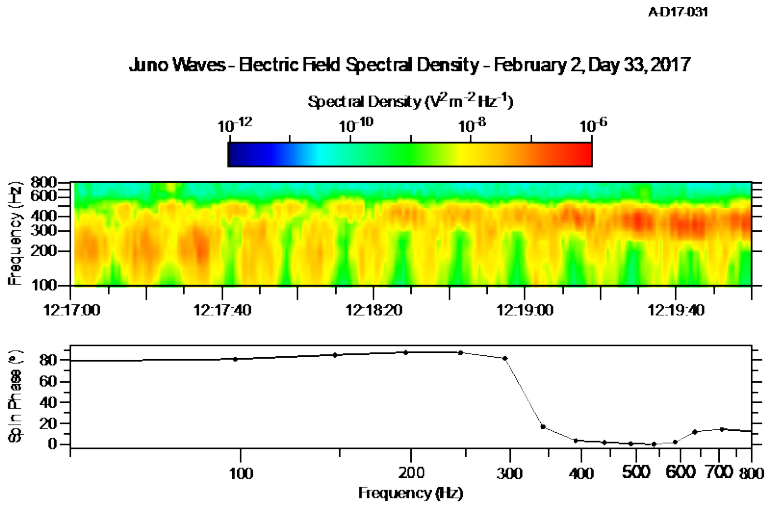

Figure 10. Top panel shows the electric field spectral density near the start of the emission on Day 033, depicting spin modulation in the electric field. The bottom panel shows the spin phase of the maximum electric field relative to the planetary magnetic field, 0 degrees representing $E \parallel B_0$, and 90 degrees representing $E \perp B_0$. The frequency-dependence in the spin phase can be seen. At lower frequencies $E \perp B_0$ and as frequency increases, the electric field becomes almost parallel to the planetary magnetic field.

earlier, the effective axis of the Waves electric antenna is oriented along the y axis, and the magnetic search coil antenna is oriented along the spacecraft z axis (see Figure 1). In the interval where these measurements were made, it turns out that the +z axis was aligned approximately perpendicular to the Jovian magnetic meridian plane. This means that twice per rotation the electric antenna measures the components of the wave electric field approximately parallel and perpendicular to the Jovian magnetic field. The top panel of Figure 9 shows an electric field spectrogram on Day 240 with a greatly expanded time scale near the edge of the left-facing funnel, from 07:52 to 07:54 UT. As can be seen, a strong spin modulation is apparent in the electric field spectral density, with alternating nulls and peaks at half the spin period. One can also see that the phase of the nulls and peaks decreases with frequency. The bottom panel of Figure 9 shows the phase relative to the

Jovian magnetic field (B_0), where a phase of 0 degrees indicates $E \parallel B_0$ and a phase of 90 degrees indicates $E \perp B_0$. As can be seen, the phase varies from about 90 degrees at low frequencies, to about 60 degrees near ~ 40 kHz. This shows that the electric field is perpendicular to the Jovian magnetic field at low frequencies, tending toward parallel as the frequency increases. An even better example of this electric field spin modulation phase shift was found on Day 033. The top panel of Figure 10 shows an electric field spectrogram on Day 033 with an expanded time scale near the edge of the right-facing funnel, from 12:17 to 12:20 UT. Again, the strong spin modulation is apparent and the phase is shown to decrease with increasing frequency. The bottom panel of Figure 10 shows the phase relative to B_0. For this pass, the phase varies from about 90 degrees at lower frequencies, to nearly 0 degrees near ~ 400 Hz. This example shows the electric field going from being perpendicular to the Jovian magnetic field to being parallel as the frequency increases.

The change in the direction of the electric field described above can be explained by the frequency dependence of the resonance cone angle, θ_{res}, which is the angle of the resonance cone relative to the magnetic field direction. The resonance cone angle is given by the following approximate equation:

$$\tan^2 \theta_{res} = -\frac{P}{S} = -\left(1 - \frac{\omega_p^2}{\omega^2}\right)$$

where P and S are defined in *Stix* [1962] and we have used the approximation $\omega_c \gg \omega_p$ which implies S ≈ 1. This equation explicitly shows that for whistler-mode waves propagating near the resonance cone the electric field direction should vary from nearly perpendicular to the magnetic field at low frequencies to more nearly parallel to the

magnetic field as the frequency increases, exactly as observed. This frequency dependent feature of the spin modulation has been previously observed for whistler-mode auroral hiss emissions at Earth, and is illustrated in Figure 8 of *Gurnett et al.* [1983] (see Figure 11). For the resonance cone angle given by the above equation to reliably give the electric field direction, the wave vector must be predominantly on one side of the resonance cone because otherwise it would average to a direction not easily related to the resonance angle. This wave vector distribution effect was previously shown via a multicomponent terrestrial study by *Santolik and Gurnett* [2002], in which a wide azimuthal distribution of wave vectors was found. For the spin modulation shown in Figure 9 for Day 240, the above condition is believed to be satisfied to a good approximation because the spacecraft at that time is located well equatorward of the magnetic field line on which the radiation is generated,

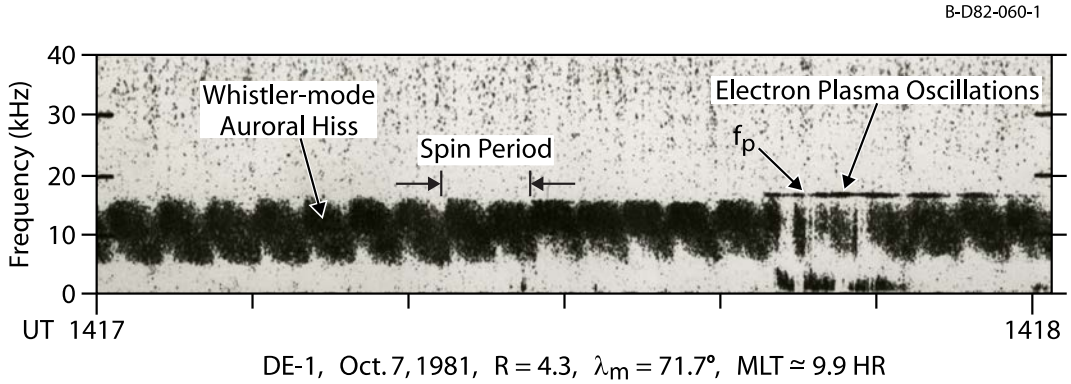

Figure 11. Figure from *Gurnett et al.* [1983] of the upper cutoff of an auroral hiss emission. The upper cutoff is the assumed plasma frequency, with electron plasma oscillations occurring at this cutoff frequency.

which is believed to be first encountered at about 08:35 UT. For the spin modulation on Day 033 shown in Figure 10, the spacecraft is leaving the source region (right-facing funnel), also providing a reliable electric field direction. Terrestrial observations of auroral hiss

(Figure 11) typically show the electric field phase angle shifting to near 0 degrees as the frequency approaches the plasma frequency. Our measurements in Figure 10 from Day 033 show this shift to near 0 degrees as frequency increases, therefore we can assume a plasma frequency near the cutoff of this emission, i.e. at about 600 Hz. Although, it is important to note a key difference between the terrestrial study from *Gurnett et al.* [1983] (Figure 11) and our current study on Day 033 (Figure 10). We do not observe electron plasma oscillations, which are clearly seen in Figure 11. These electron plasma oscillations indicate the exact location of the plasma frequency. Because Juno Waves did not observe these oscillations on Day 033, our assumed plasma frequency is an estimate. As for our measurements from Day 240, shown in Figure 9, only a phase shift to about 50 degrees is shown. The reason why the phase shift does not extend to near 0 degrees appears to be due to the fact that emission does not extend all the way up to the plasma frequency.

CHAPTER 5

ORIGIN OF THE RADIATION

Whistler-mode plasma wave emissions can originate either from a remote source elsewhere in the magnetosphere, or from a local source. A common source for whistler-mode auroral hiss at Earth is an electron beam, which was first quantitatively studied by *Gurnett* [1966]. In order to see if the plasma wave emissions are generated by electron beams we compared the Waves data from each pass with particle measurements from the Jupiter Energetic particle Detector Instrument (JEDI) [*Mauk et al.*, 2013]. For each pass, an upward-going electron beam was detected by JEDI [*Mauk et al.*, 2017] over similar time intervals as the emissions observed by Waves. It should be noted that the energies of the upward-going electron are a few orders of magnitude higher than those previously observed at Earth (typically hundreds of eV). However, at the outer planets, such as Saturn, electron energies associated with auroral hiss have been detected on the order of hundreds of keV [*Mitchell et al.*, 2005], consistent with the electron energies this study has observed. The top two panels in Figure 12 (Day 240), 13 (Day 346), and 14 (Day 033) show plots of the upward-going electron fluxes with pitch angles from 0 to 15 degrees (energies of $\sim$25 to $>$800 keV) from JEDI and the Waves electric field spectral density data (frequency range of 10^3 to 10^4 Hz). Upon initial visual analysis, the electron beams and the electric field data seem to have similar upward-going trends, which is especially noticeable for Day 240 (Figure 12), and corresponding peaks and valleys. An especially striking characteristic from Day 346 (Figure 13) occurs around 15:40 UT, where the electron fluxes from JEDI have a clear spike and correlate with spectral density in electric field from Waves occurring at the same time. To test whether the whistler-mode emissions are generated by the electron

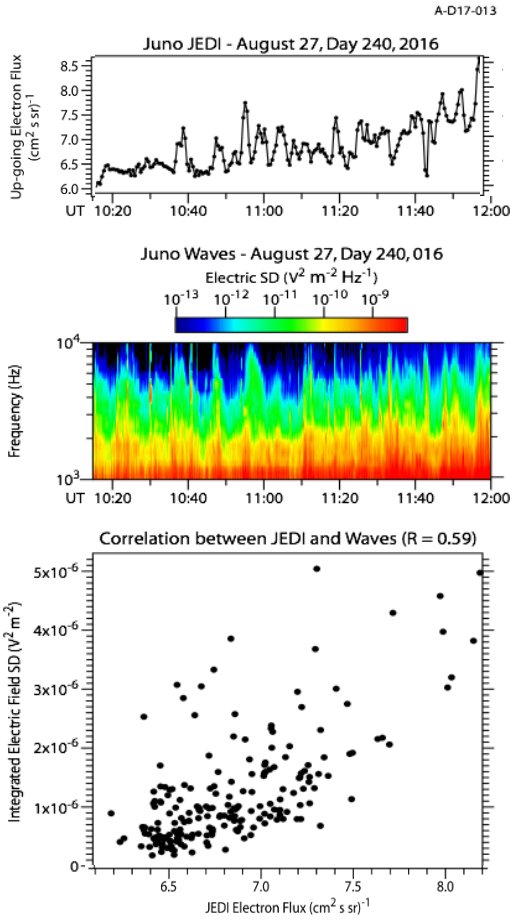

Figure 12 (left). Top panel shows the up-going JEDI electron fluxes with pitch angles between 0 and 15 degrees and with energies of ~25 to > 800 keV for Day 240. The second panel shows the Waves electric field spectral density for frequencies between 10^3 and 10^4 Hz. Similar upward trends are seen in both the JEDI and Waves data as well as matching times corresponding to peaks and valleys in the two data sets. The bottom panel shows the JEDI electron fluxes plotted versus the integrated electric field spectral density from Waves (integrated over $10^3 - 10^4$ Hz). A high correlation corresponds to a positively-sloped linear fit. The correlation coefficient (R) was calculated for the two datasets and found to be about 0.59.

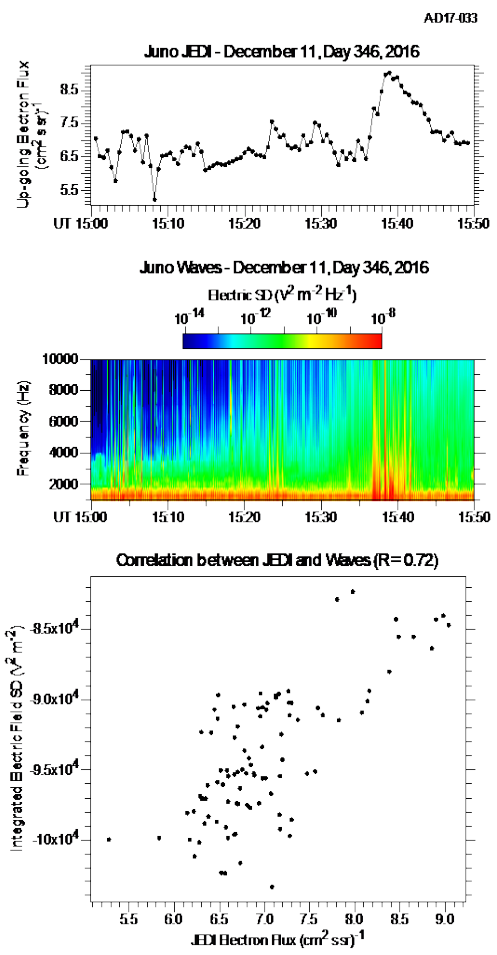

Figure 13 (right). Top panel shows the up-going JEDI electron fluxes with pitch angles between 0 and 15 degrees and with energies of ~25 to > 800 keV for Day 346. The second panel shows the Waves electric field spectral density for frequencies between 10^3 and 10^4 Hz. Similar upward trends are seen in both the JEDI and Waves data as well as matching times corresponding to peaks and valleys in the two data sets, especially around 15:40 UT. The bottom panel shows the JEDI electron fluxes plotted versus the integrated electric field spectral density from Waves (integrated over $10^3 - 10^4$ Hz). A high correlation corresponds to a positively-sloped linear fit. The correlation coefficient (R) was calculated for the two datasets and found to be about 0.72.

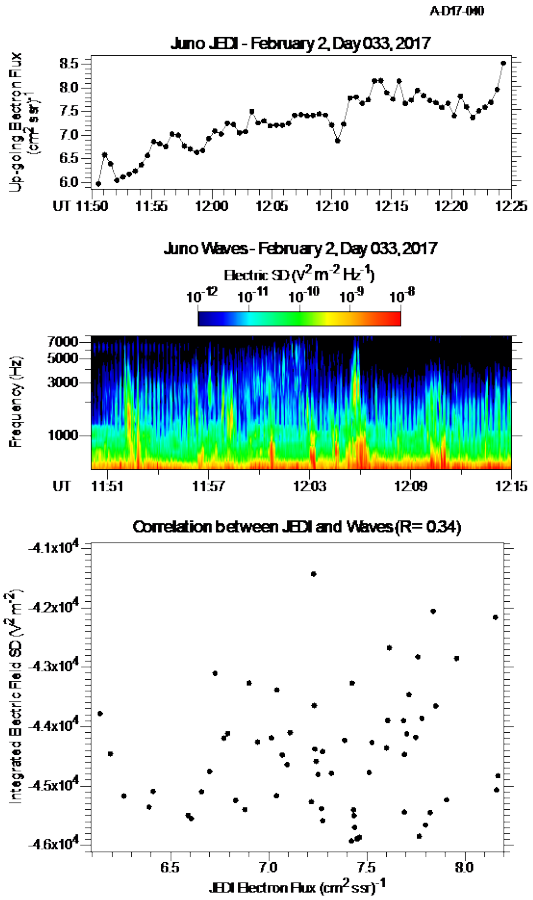

Figure 14. Top panel shows the up-going JEDI electron fluxes with pitch angles between 0 and 15 degrees and with energies of ~ 25 to > 800 keV for Day 033. The second panel shows the Waves electric field spectral density for frequencies between 10^3 and 10^4 Hz. Similar upward trends are seen in both the JEDI and Waves data as well as matching times corresponding to peaks and valleys in the two data sets. The bottom panel shows the JEDI electron fluxes plotted versus the integrated electric field spectral density from Waves (integrated over $10^3 - 10^4$ Hz). A high correlation corresponds to a positively-sloped linear fit. The correlation coefficient (R) was calculated for the two datasets and found to be about 0.34.

beams, we performed cross-correlations. The electron fluxes were plotted against the integrated electric field strength, shown as scatter plots in the bottom panels of Figure 12, 13, and 14. All three plots show clear upward linear trends. To determine the significance of each visual linear correlation, we computed the correlation coefficients (with 1 indicating a perfect correlation). For Day 240, the correlation coefficient was found to be 0.59, for Day

346 it was 0.72, and 0.34 for Day 033. All three were indicative of a significant correlation, although Day 346 had the highest correlation and Day 033 had the lowest. The significance of each correlation was calculated, using a chi-squared test, based on the probability that a random distribution with N pairs of data points would produce such correlation coefficient values. For both Day 240 and Day 346 the probability was less than 0.000001 and for Day 033 the probability was calculated as approximately 0.00398. Each calculation was based on the particular correlation and N value for each day. Although the probability for Day 033 was higher than the other two days, it is still a relatively low probability and therefore we consider our calculated correlation coefficient values to be significant. These correlations provide evidence that the emissions are in fact due to electron beams and we therefore assume they are generated by up-going electron beams.

Another important clue supporting this generation mechanism is shown in Figure 7. The red and black dots represent the time periods corresponding to the lower-frequency cutoffs at the start and end of each emission. Upon visual analysis, these dots seem to overlap the edges of the statistical auroral oval. Not only do these time periods correspond to our observed emissions, but intensifications in the up-going electron fluxes were found in the JEDI data at similar times, also mapping to the statistical auroral oval [*Mauk et al.*, 2017]. This provides further evidence that these whistler-mode wave emissions are generated by up-going electron beams originating from the Jovian polar cap region.

Experimental studies have shown clear evidence that electron beams can generate whistler-mode auroral hiss emissions. In a 1986 study, done on the Spacelab 2 mission, an artificial electron beam was ejected from an electron gun onboard a space shuttle and was detected by the Plasma Diagnostic spacecraft, supporting the idea of an electron beam being

the source of the whistler-mode auroral hiss emissions observed near Earth, as shown in Figure 15 [*Gurnett et al.*, 1986]. Two proposed theories for the local generation of whistler-mode emissions are incoherent and coherent processes, the latter relating to a plasma instability. The difference between the two theories has to do with the number of particles involved in the interaction. A coherent mechanism deals with a lot of particles acting in phase to generate the emission. The power that comes out of a coherent generation process goes as N^2, where N is the total number of particles. In contrast, incoherent mechanisms

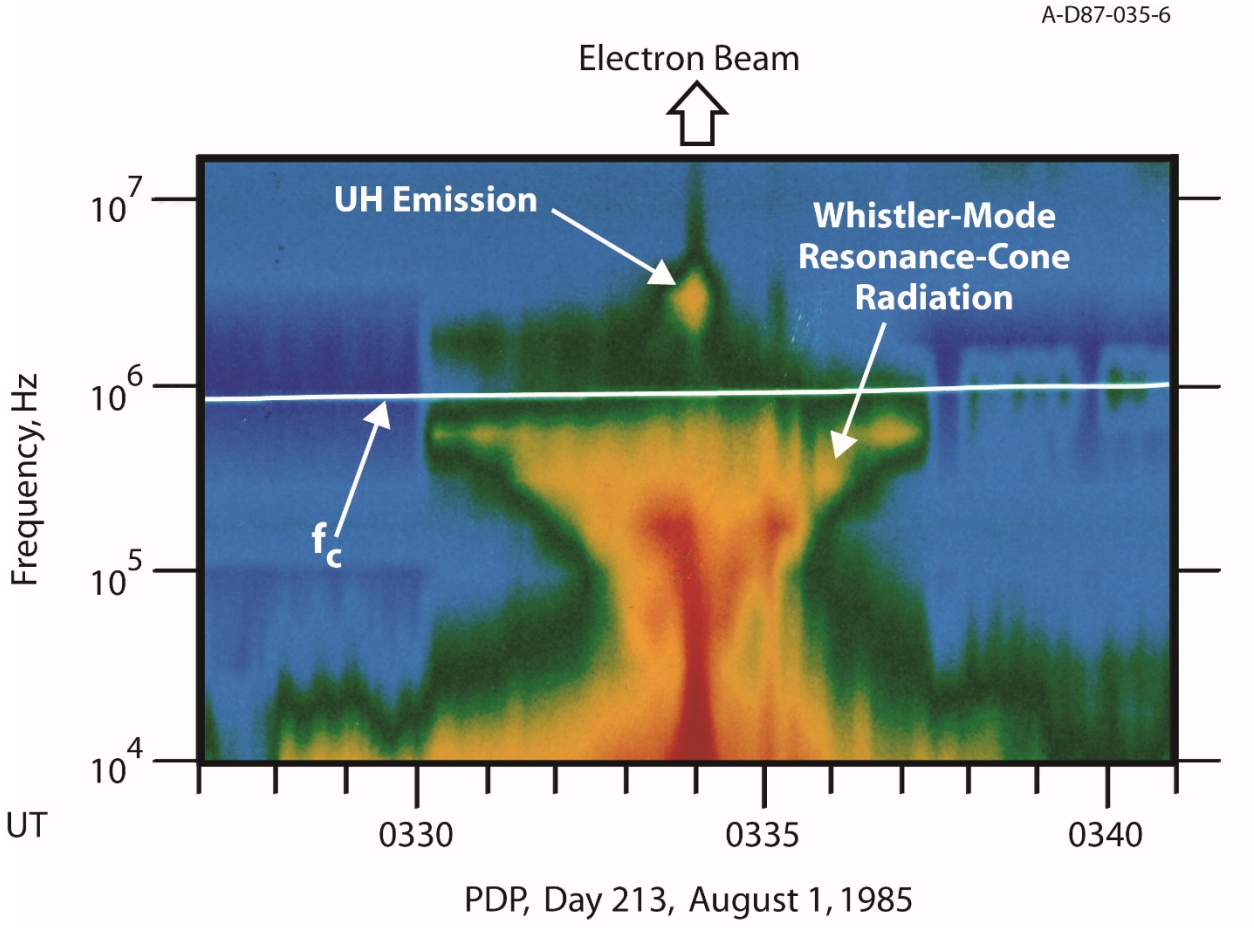

Figure 15. A frequency-time spectrogram adopted from *Gurnett et al.* [1986] and *Farrell et al.* [1988] from the PDP plasma wave instrument. The emissions were detected during a dc electron gun firing. Whistler-mode emissions are detected, where the frequency extends up to the electron cyclotron frequency.

deal with individual particles not acting in phase. The power that comes from incoherent sources is proportional to *N* because the power from each particle is added together [*Farrell et al.*, 1988]. Many early studies were based on the incoherent generation of whistler-mode auroral hiss via Cerenkov radiation [*Ellis*, 1959; *Liemohn*, 1965; *Jorgensen*, 1968]. Cerenkov radiation occurs when the particles within a plasma move faster than the phase velocity of the wave. This can occur if the index of refraction is greater than one, such as near the resonance cone. This incoherent process for terrestrial auroral hiss was later dismissed by *Taylor and Shawhan* [1974] because of its inability to explain the amplitude of the observed emissions. Later, the idea of a coherent beam-to-plasma interaction near the Landau resonance velocity was proposed by *Maggs* [1976]. Using a computer simulation, *Farrell et al.* [1989] showed that whistler-mode emission can be produced by this beam-to-plasma instability. The instability is associated with the Landau resonance in which an unstable wave increases its energy when it interacts with particles. The coherent generation mechanism was also experimentally tested for its accuracy by a later study on the Spacelab 2 electron beam experiment [*Farrell et al.*, 1998]. This study found that the measured wave powers were greater than were expected from incoherent Cerenkov radiation and therefore must be generated by a coherent plasma instability. Hence, coherent plasma instabilities are currently the assumed local generation mechanisms for whistler-mode emissions. Therefore, we conclude that our observed whistler-mode wave emissions are generated by up-going electron beams, which are ultimately caused by a coherent plasma instability, often called a "beam-plasma instability".

CHAPTER 6

SUMMARY

This paper has investigated the characteristics of new plasma wave emissions observed by the Juno spacecraft over the high latitude regions of Jupiter's magnetosphere. The emissions were seen on three days corresponding to three passes: PJ1 on Day 240 of 2016, PJ3 on Day 346 of 2016, and PJ4 on Day 033 of 2017. The emissions observed show signatures in both the electric and magnetic fields, indicating that the waves are electromagnetic waves. The spectrum's relation to the characteristic frequencies of the plasma show that the electron cyclotron frequency is well above the frequencies of the observed plasma wave emissions for all three days for the entire duration of each pass. The emissions also have one-half of a characteristic funnel-shape and show similarities to whistler-mode auroral hiss emissions previously observed near Earth. The plasma frequency was assumed for each day based on the conclusion that the emissions are propagating in the whistler-mode and frequency-dependent electric field spin modulations, similar to whistler-mode auroral hiss studies from Earth. However, even though the phase shifts in the spin modulation were only detected on two of the three days (Day 240 and Day 033), we still assume that all three emissions are propagating in the whistler-mode because of the similarities between each emission. It was also found that the estimated plasma frequency for Day 240 was much higher than that for Day 033. This is due to the location of the spacecraft. Another characteristic that was analyzed was the electric to magnetic field ratio. It was found that these ratios were approximately three near the start of the emission, then decrease to about one for the remaining duration of the passes. There were higher ratios observed for both Day 346 and Day 033 than on Day 240, but all three days showed similar

trends throughout the emissions, including the lower ratios throughout the bulk of the emissions. It has been shown that the whistler-mode can demonstrate characteristics similar to a nearly isotropic free-space mode when the cyclotron frequency is very high. However, at large wave normal angles, such as near the resonance cone, the *E/cB* ratio can become much greater than one.

The possible origins of the whistler-mode emissions were analyzed by performing cross-correlation tests between the flux of up-going electron beams, observed by JEDI, and the integrated Waves electric field spectral densities. Significant correlations were found with correlation coefficients of 0.59, 0.72, and 0.34 for Day 240, Day 346, and Day 033 respectively. It was also found that the lower-frequency cutoffs of the emissions correspond to time periods in which Juno passes over the statistical auroral oval and when JEDI detected intensifications in electron flux. It is believed that the observed plasma wave emissions are propagating in the whistler-mode due to plasma instabilities driven by beams of up-going electrons along the polar cap region.

Through this study and future studies from Juno spacecraft observations, the dynamics of the Jovian magnetosphere and generation mechanisms of auroral-related phenomenon will be further understood. This work helps to compare whistler-mode emissions on Jupiter to terrestrial observations of auroral hiss. Not only will this work aid in understanding the theories behind whistler-mode emissions, but models of the Jovian magnetosphere will be greatly improved. One vital application of this study is to better understand the Jovian current system. An equilibrium is needed, therefore downward currents, to close the observed upward currents in the auroral zone [*Bagenal et al*., 2014]. Currently, the location of these downward currents is unknown. Since this study has shown

correlation with up-going electrons in the polar cap region, this may indicate a location of these downward current regions. However, the current magnetic field models have been shown to be very inaccurate and need significant improvement. This study can provide better estimates of the local electron plasma frequency, and ultimately the density contours, in the polar regions. The current field models can then be improved and used to determine where the field lines these emissions are detected on map to, whether that be in the plasmasheet or the deeper in the magnetotail. Overall, this study will be extended to help answer these questions regarding the Jovian current system and current magnetic field models.

REFERENCES

Bagenal, F. (1992), Giant Planet Magnetospheres, *Annu. Rev. Earth Planet. Sci.*, 20:289-328.

Bagenal, F. et al. (2014), Magnetospheric science objectives of the Juno mission, *Space Sci. Rev.*, doi:10.1007/s11214-014-0036-8.

Bigg, E. K. (1964), Influence of the satellite Io on Jupiter's decametric emission, *Nature*, 203:1008-10.

Bolton, S. J., and the Juno Science Team (2010), The Juno Mission, *International Astronomical Union 2010*, doi:10.1017/S1743921310007313.

Burke, B. F., and K. L. Franklin (1955), Observations of a variable radio source associated with the planet Jupiter, *J. Geophys. Res.*, doi:10.1029/JZ060i002p00213.

Carr, T. D., M. D. Desch, and J. K. Alexander (1983ba), Phenomenology of magnetospheric radio emissions, *Physics of the Jovian magnetosphere*, A83-26611 10-91, Cambridge and New York, Cambridge University Press, p. 226-284.

Connerney, J. E. P., M. H. Acuña, N. F. Ness, and T. Satoh (1998), New models of Jupiter's magnetic field constrained by the Io flux tube footprint, *J. Geophys. Res. Space Physics*, 103(A6), 11, 929-11, 939, doi:10.1029/97JA03726.

Connerney, J. E. P. et al. (2017), The Juno Magnetic Field Investigation, *Space Sci. Rev.*, doi:10.1007/s11214-017-0334-z.

Drake, F. D. and Hvatum, S. (1959), *Astron. J.*, 64, 329.

Ellis, G. R. A. (1959), Low-frequency electromagnetic radiation associated with magnetic disturbances, *Planet. Space Sci.*, 1, 253-254, doi:10.1016/0032-0633(59)90029-7.

Ergun, R. E., et al. (2003), Fast auroral snapshot satellite observations of very low frequency saucers, *Physics of Plasmas*, 10(2), doi:10.1063/1.1530160.

Farrell, W. M., D. A. Gurnett, P. M. Banks, R. I. Bush, and W. J. Raitt (1988), An analysis of whistler mode radiation from the Spacelab 2 electron beam, *J. Geophys. Res.*, 93(A1), 153-161, doi:10.1029/JA093iA01p00153.

Farrell, W.M., D.A. Gurnett, and C.K. Goertz (1989), Coherent Cherenkov radiation from the Spacelab 2 electron beam, *J. Geophys. Res.*, 94, 443.

Farrell, W.M., et al. (1993), An interpretation of the broadband VLF waves near the Io torus as observed by Ulysses, *J. Geophys. Res.*, 98, 21,177-21,188.

Farrell, W.M., et al. (1998), A simple simulation of a plasma void: Applications to Wind observations of the lunar wake,

Field, G. B. (1959), The source of radiation from Jupiter at decimeter wavelengths, *J. Geophys. Res.*, doi:10.1029/JZ064i009p01169.

Gurnett, D. A., and B. J. O'Brien (1964), High-latitude geophysical studies with satellite Injun 3, 5. Very low frequency electromagnetic radiation, *J. Geophys. Res.*, 69(1), 65.

Gurnett, D. A. (1966), A satellite study of VLF hiss, *J. Geophys. Res.*, 71(23), 5599-5615, doi:10.1029/JZ071i023p05599.

Gurnett, D. A., S. R. Mosier, and R. R. Anderson (1971), Color spectrograms of very-low-frequency Poynting flux data, *J. Geophys. Res.*, 76(13), 3022.

Gurnett, D. A. and L. A. Frank (1976), Continuum radiation associated with low-energy electrons in the outer radiation zone, *J. Geophys. Res.*, 81, 3875-3885, 1976 AGU.

Gurnett, D.A., W.S. Kurth, and F.L. Scarf (1979), Auroral hiss observed near the Io plasma torus, *Nature*, 280, 767-770, doi:10.1038/280767a0.

Gurnett, D. A., S. D. Shawhan, and R. R. Shaw (1983), Auroral hiss, Z mode radiation, and auroral kilometric radiation in the polar magnetosphere: DE 1 observations, *J. Geophys. Res.*, 88(A1), 329-340, doi:10.1029/JA088iA01p00329.

Gurnett, D. A., W. S. Kurth, J. T. Steinberg, P. M. Banks, R. I. Bush, and W. J. Raitt (1986), Whistler-mode radiation from the Spacelab 2 electron beam, *Geophys. Res. Lett.*, 13(3), 225-228, doi:10.1029/GL013i003p00225.

Gurnett, D. A. et al. (2005), Radio and plasma wave observations at Saturn from Cassini's approach and first orbit, *Science*, 307, 1255-1259, doi:10.1126/science.1105356.

Gurnett, D. A., and A. Bhattacharjee (2005), *Introduction to Plasma Physics with Space and Laboratory Applications*, Cambridge University Press, Cambridge, UK.

James, H. G. (1976), VLF saucers, *J. Geophys. Res.*, 81, 501-514, doi:10.1029/JA081i004p00501.

Jorgensen, T. S. (1968), Interpretation of auroral hiss measured on OGO-2 and at Byrd Station in terms of incoherent Cherenkov radiation, *J. Geophys. Res.*, 73(3), 1055-1069, doi:10.1029/JA073i003p01055.

Kennel, C. F. (1972), Stably trapped proton limits for Jupiter, In *Proc. Of the Jupiter Radiation Belt Workshop*, ed. A. J. Beck, pp. 347-361, NASA Tech. Memo 33-543, Jet Propulsion Laboratory, Pasadena, California.

Kurth, W. S. et al. (2017), The Juno Waves investigation, *Space Sci. Rev.*, submitted.

Laaspere, T., W. C. Johnson, and L. C. Semprebon (1971), Observations of auroral hiss, LHR noise, and other phenomena in the frequency range 20 Hz to 540 kHz on Ogo 6, *J. Geophys. Res.*, 76, 4477.

Liemohn, H. B. (1965), Radiation from electrons in magnetoplasma, *Radio Sci. J. of Research NBS/USNC-URSI*, 69D(5), 741-765, doi:10.6028/jres.069D.084.

Lin, C. S., J. L. Burch, S. D. Shawhan, and D. A. Gurnett (1984), Correlation of auroral hiss and upward electron beams near the polar cusp, *J. Geophys. Res.*, 89(A2), 925.

Maggs, J. E. (1976), Coherent generation of VLF hiss, *J. Geophys. Res.*, 80(10), 1707-1724, doi:10.1029/JA081i010p01707.

Martin, L.H., R.A. Helliwell, and K.R. Marks (1960), Association between aurorae and very low-frequency hiss observed at Byrd Station, Antarctica, *Nature*, 187(4739), 751.

Mauk, B. H., et al. (2013), The Jupiter Energetic Particle Detector Instrument (JEDI) Investigation for the Juno Mission, *Space Sci. Rev.*, pp. 1-58, 10.1007/s11214-013-0025-3.

Mauk, B. H., et al. (2017), Juno observations of energetic charged particles over Jupiter's polar regions: Analysis of mono- and bi-directional electron beams, *Geophys. Res. Lett.*, doi: 10.1002/2016GL072286.

McDonald, F. B., and J. H. Trainor (1976), Observations of energetic Jovian electrons and protons, in *Jupiter*, edited by T. Gehrels, p. 961, University of Arizona Press, Tucson.

McEwen, D. J., and R. E. Barrington (1967), Some characteristics of the lower hybrid resonance noise bands observed by the Alouette 1 satellite, *Can. J. Phys.*, 45, 13.

Mitchell, D. G., et al. (2005), Energetic ion acceleration in Saturn's magnetotail: substroms at Saturn?, *Geophys. Res. Lett.*, 32, L20S01, doi:10.1029/2005GL022647.

Moses, S. L., F. V. Coroniti, C. F. Kennel, W. S. Kurth, and D. A. Gurnett (1990), Comparison of plasma wave measurements in the bow shocks at Earth, Jupiter, Saturn, Uranus, and Neptune, *Geophys. Res. Lett.*, 17, 1653-1656.

Mosier, S. R., and D. A. Gurnett (1969), VLF measurements of the Poynting flux along the geomagnetic field with the Injun 5 satellite, *J. Geophys. Res.*, 74(24), 5675-5687, doi:10.1029/JA074i024p05675.

Santolik, O., and D. A. Gurnett (2002), Propagation of auroral hiss at high altitudes, *Geophys. Res. Lett.*, 29(10), 1481, doi:10.1029/2001GL01366.

Scarf, F. L., D. A. Gurnett, and W. S. Kurth (1979), Jupiter plasma wave observations: An initial Voyager 1 overview, *Science*, 204(4396), 991-995, doi:10.1126/science.204.4396.991.

Simpson, J. A., D. Hamilton, G. Lentz, R. B. McKibben, A. Mogro-Campero, M. Perkins, K. R. Pyle, A. J. Tuzzolino, and J. J. O'Gallagher (1974*a*), Protons and electrons in Jupiter's magnetic field, results from the University of Chicago experiment on Pioneer 10, *Science*, 183, 306.

Simpson, J. A., D. C. Hamilton, G. A. Lentz, R. B. McKibben, M. Perkins, K. R. Pyle, A. J. Tuzzolino, and J. J. O'Gallagher (1975), Jupiter revisited: First results from the University of Chicago charger particle experiment on Pioneer 11, *Science*, 188, 455.

Smith, R. L. (1969), VLF observations of auroral beams as sources of a class of emissions, *Nature*, 224(5217), 351-352, doi:10.1038/224351a0.

Stix, T. H. (1962), *The Theory of Plasma Waves*, McGraw-Hill, New York.

Taylor, W. W. L., and S. D. Shawhan (1974), A test of incoherent Cerenkov radiation for VLF hiss and other magnetospheric emissions, J. Geophys. Res., 79(1), 105-117, doi:10.1029/JA079i001p00105.

Tetrick, S. S., D. A. Gurnett, W. S. Kurth, M. Imai, G. B. Hospodarsky, S. J. Bolton, J. E. P. Connerney, S. M. Levin, and B. H. Mauk (2017), Plasma waves in Jupiter's high-latitude regions: Observations from the Juno spacecraft, Geophys. Res. Lett., 44, doi:10.1002/2017GL073073.

Thorne, R. M., and F. V. Coroniti (1972), A self consistent model for Jupiter's radiation belts, In *Proc. Of the Jupiter Radiation Belt Workshop*, p. 363-380, ed. A. J. Beck, NASA JPL TM 33-543, Jet Propulsion Laboratory, Pasadena, California.

Van Allen, J. A., G. H. Ludwig, E. C. Ray, and C. E. McIlwain, Observations of High Intensity Radiation by Satellites 1958 Alpha and Gamma (1958), *Jet Propulsion 28, 588-592.*

Van Allen, J. A., D. N. Baker, B. A. Randall, and D. D. Sentman (1974*b*), The magnetosphere of Jupiter as observed with Pioneer 10, 1, Instrument and principal findings, *J. Geophys. Res.*, 79, 3559.

Van Allen, J. A., B. A. Randall, D. N. Baker, C. K. Goertz, D. D. Sentman, M. F. Thomsen, and H. R. Flindt (1975), Pioneer 11 observations of energetic particles in the Jovian magnetosphere, *Science*, 188, 459.